Changes in intra-nuclear mobility of mature snRNPs provide a mechanism for splicing defects in Spinal Muscular Atrophy.

Allyson Kara Clelland, Alexandra Beatrice Elizabeth Bales, Judith Elizabeth Sleeman, University of St Andrews, School of Biology, MBSB North Haugh, St Andrews, Fife, KY16 9TF, UK.

Corresponding author: Judith Sleeman, University of St Andrews, School of Biology, MBSB North Haugh, St Andrews, Fife, KY16 9TF, UK.
Tel: +44 1334 463524
Fax: +44 1334 463600
jes14@st-andrews.ac.uk

Condensed title: Altered snRNP dynamics in SMA

word count 7340

JCS online publication date 19 April 2012

Summary

It is becoming increasingly clear that defects in RNA metabolism can lead to disease. Spinal Muscular Atrophy (SMA), a leading genetic cause of infant mortality, results from insufficient amounts of survival motor neuron (SMN) protein. SMN is required for the biogenesis of snRNPs: essential components of the spliceosome. Splicing abnormalities have been detected in models of SMA but it is unclear how lowered SMN affects the fidelity of pre-mRNA splicing. We have examined the dynamics of mature snRNPs in cells depleted of SMN and demonstrated that SMN depletion increases the mobility of mature snRNPs within the nucleus. To dissect the molecular mechanism by which SMN deficiency affects intra-nuclear snRNP mobility, we employed a panel of inhibitors of different stages of pre-mRNA processing. This in vivo modeling demonstrates that snRNP mobility is altered directly as a result of impaired snRNP maturation. Current models of nuclear dynamics predict that sub-nuclear structures, including the spliceosome, form by self-organization mediated by stochastic interactions between their molecular components. Thus, alteration of the intra-nuclear mobility of snRNPs provides a molecular mechanism for splicing defects in SMA.

Introduction

The spliceosome is a multi-component molecular machine responsible for the catalysis of pre-mRNA splicing. The organization of the spliceosome within mammalian cell nuclei is a complex and dynamic process. Splicing snRNPs (small nuclear ribonuceoproteins) form the core of the spliceosome. The major spliceosome comprises U1, U2, U5, U4/U6 snRNPs, while in the minor spliceosome U1 and U2 are replaced by U11 and U12 (Tarn and Steitz, 1996). Each snRNP comprises a core of uridine-rich small nuclear RNA (U1, U2, U5, U4/U6, U11, U12) complexed with the seven Sm proteins (Sm B/B', D1, D2, D3, E, F and G) and other proteins specific to each snRNP (reviewed in Will and Luhrmann, 2001). Splicing snRNPs have a complex pattern of localization within the cell, reflecting their complex biogenesis. With the exception of U6, whose biogenesis is thought to be entirely nuclear (reviewed in Patel and Bellini, 2008), snRNAs are transcribed by RNA PolII in the nucleus then exported to the cytoplasm where the Sm proteins are assembled into a ring structure around the snRNA (Kambach et al., 1999; Stark et al., 2001). This process is co-ordinated and controlled by the survival of motor neurons (SMN) complex (reviewed in Battle et al., 2006; Chari et al., 2009). Decreased amounts of SMN protein lead to the inherited neurodegenerative condition, Spinal Muscular Atrophy (SMA). Following the assembly of the Sm core, the 5' cap of the U snRNA becomes hypermethylated and the 3' end is trimmed before the partially mature snRNP can be reimported into the nucleus. On entry into the nucleus, snRNPs accumulate in Cajal bodies (Carvalho et al., 1999; Sleeman and Lamond, 1999) where their maturation continues (reviewed in Cioce and Lamond, 2005). In many, but not all, cells Cajal bodies co-localize with their twin structures, gems (Gemini of Cajal bodies) that contain the SMN protein (Liu and Dreyfuss, 1996). Cajal bodies are also implicated in the recycling of snRNPs after spliceosome disassembly (Schaffert et al., 2004; Sleeman, 2007; Stanek et al., 2008; Stanek et al., 2003). Mature splicing snRNPs localize to nuclear speckles (also termed interchromatin granules clusters (IGCs)), which are thought to provide a reservoir of mature snRNPs for recruitment to active spliceosomes when needed (reviewed in Spector and Lamond, 2011). Various strategies for modelling the kinetic behaviour of snRNPs and other pre-mRNA splicing factors suggest that splicing factors are in constant dynamic exchange in and out of speckles and that the speckles form by self-organization dependant on the dynamic interactions of their components (reviewed in Iborra and Cook, 2002; Misteli, 2001a, b, 2010). The active

spliceosome itself is also proposed to be a self-organizing structure formed as a result of stochastic interactions between individual protein and RNA components (reviewed in Rino and Carmo-Fonseca, 2009). Since the movement of splicing factors and other proteins within the nucleus occurs by anomalous diffusion with their movement slowed by transient binding to specific sites of biological importance (Kruhlak et al., 2000; Phair and Misteli, 2000; Rino et al., 2007), the intra-nuclear dynamics of snRNPs reflect the balance of their activity in spliceosomes and storage in speckles.

The inherited neurodegenerative condition SMA, one of the leading genetic causes of infant mortality, is caused by lowered levels of the SMN protein with the degree of reduction of SMN showing some correlation with the severity of symptoms (Coovert et al., 1997; Lefebvre et al., 1997). Despite the well-defined role for SMN in early cytoplasmic stages of splicing snRNP assembly, the mechanism by which SMN reduction leads to symptoms of motor neuron loss and subsequent muscle degeneration is unknown. It is unclear whether motor neurons are particularly sensitive to defects in splicing snRNP maturation or whether SMN has an additional motor neuron-specific function. A comparison of mouse models of SMA exhibiting differing phenotypic severities revealed a correlation between the degree of impairment of snRNP assembly and the severity of symptoms (Gabanella et al., 2007). Cell type-specific and snRNP-specific alterations in the repertoire of snRNAs have been detected in severe SMA mice and in HeLa cells showing 15% or less of normal SMN levels (Gabanella et al., 2007; Zhang et al., 2008). Widespread defects in splicing were also detected in severe SMA mice leading to the proposal that changes in the stochiometry of snRNPs may result in splicing abnormalities by affecting the efficiency, rate and fidelity of spliceosome assembly on different introns (Zhang et al., 2008) with important motor neuron-specific transcripts preferentially affected. Defects in splicing events mediated by both the minor and the major spliceosomes have been identified in cells from SMA patients with 40-50% of normal SMN levels (Boulisfane et al., 2011; Fox-Walsh and Hertel, 2009; Wan et al., 2005) while SMN-deficient fission yeast also show splicing defects consistent with inefficient spliceosome formation (Campion et al., 2010). To date, however, no key neural transcripts affected by SMN-depletion in mammals have been identified and the molecular mechanism linking an altered snRNP repertoire to the varied and widespread splicing defects seen is not clear. We have examined the effect of SMN reduction on the

localization and dynamics of splicing snRNPs in a human neural cell line and in fibroblasts from an SMA patient. Our data reveal significant alterations in the rates of movement of snRNPs within the nuclei of SMN-depleted cells that provide a possible mechanistic link between defects in ribonucleoprotein assembly and defects in splicing.

Results

1) SMN can be reduced effectively by RNAi in HeLa and SH-SY5Y cells.

It is well established that lowered levels of SMN result in the loss of SMN from nuclear gems and defects in splicing snRNP maturation (Clelland et al., 2009; Girard et al., 2006; Gonsalvez et al., 2007; Lemm et al., 2006; Shpargel and Matera, 2005). In order to investigate the effect of decreased levels of SMN on the structure of splicing factor speckles and on the dynamics of mature splicing snRNPs, we identified siRNA sequences capable of reducing SMN levels in HeLa cells and in the neuroblastoma cell line SH-SY5Y. Transient transfection of HeLa cells with two independent siRNA duplexes to SMN (SMN 01 and SMN 05) led to a dramatic reduction in the number of SMN-positive nuclear gems after 24 hrs in comparison to cells transfected with non-targeting duplexes or control duplexes targeting lamin A/C (Fig. 1A,B). Transfection of SH-SY5Y cells with siRNA duplexes to SMN resulted in a reduction to 48% of normal SMN protein levels after 24 hrs and 32% of normal after 48 hrs (Fig. 1 C,D) compared to transfection with non-targeting duplexes or control duplexes targeting PPIB.

2) SMN reduction can be achieved using expression of shRNAs

We have previously demonstrated that the neuroblastoma cell line, SH-SY5Y, has relatively low endogenous levels of SMN with a small over-expression of SMN able to increase the rate of accumulation of newly-assembled snRNPs in nuclear speckles (Clelland et al., 2009). This cell line is an ideal model in which to study the effect of SMN reduction on mature snRNPs because it is the level of SMN that limits the splicing snRNP assembly pathway in SH-SY5Y cells. In order to investigate the dynamics of mature snRNPs in SMN-depleted SH-SY5Y cells, it was essential to unequivocally identify living cells with lowered levels of SMN. To achieve this, we used the sequence identified above as capable of reducing SMN levels to generate plasmids to express small hairpin RNAs (shRNAs) from an H1 promoter with GFP expressed from a PGK promoter on the same plasmid (pSuperGFP, oligoengine). SH-SY5Y cells were transfected with these vectors and assayed for SMN expression after 24, 48 and 72 hours by indirect immunofluorescence using antibodies to SMN. Transfected SH-SY5Y cells, identified by expression of GFP, showed reduced SMN levels after 48 hours of shRNA expression (Fig. 2A,B,C). This reduction was also evident at 72 hours. Expression of a control plasmid expressing shRNAs to target PPIB had no effect on SMN levels or distribution (Fig. 2D). Quantitation of the SMN fluorescence signal 48 hours after

transfection with plasmids targeting SMN reveals a reduction to an average of 46% of normal SMN levels in whole cells and to an average of 56% of normal SMN in nuclei (Fig. 2E). These data demonstrate that shRNA expression can efficiently reduce SMN in SH-SY5Y cells to levels comparable to those seen in cells from SMA patients, but that longer incubation is required in comparison to direct transfection of siRNA duplexes. Furthermore the loss of SMN appears to be more pronounced in the cytoplasm than in the nucleus.

3) Reduction of SMN does not disrupt the structure of splicing speckles

Depletion of SMN has been demonstrated to lead to inefficient snRNP assembly (reviewed in Pellizzoni, 2007) and to a delay in newly assembled snRNPs reaching splicing factor speckles (Girard et al 2006). However, the effect of SMN depletion on nuclear speckles containing mature splicing factors has not been examined in detail. Although the level of SMN available is the limiting factor in the rate of snRNP accumulation in speckles in SH-SY5Y neuroblastoma cells (Clelland et al., 2009), reduction of SMN levels using shRNA expression does not cause an appreciable defect in the localization of steady-state splicing factors in speckles (Fig. 3). The SR domain splicing factor SC-35 (A), core snRNP Sm proteins (B), the U1 snRNP-specific protein U1A (C) and snRNAs, detected using an antibody to their tri-methyl guanosine cap (D), all show normal localization in SH-SY5Y cells depleted of SMN for 48hrs (compare transfected cells, green on overlay, with control cells in the same panel). It is notable, however, that SH-SY5Y cells show accumulations of TMG-capped snRNAs in their cytoplasm (arrows in D), suggesting that snRNP assembly is less efficient in these cells than in HeLa cells where such accumulations are not seen (Carvalho et al., 1999; Sleeman et al., 2003).

4) Mature snRNPs show alterations in their dynamics in cells depleted of SMN.

Because the spliceosome is believed to assemble by self-organization, it is important to address the intra-nuclear dynamics of splicing factors in addition to their steady-state distribution. In order to study the dynamics of splicing snRNPs in SMN-depleted cells, we first established cell lines constitutively expressing mCherry-tagged SmB. mCherry-SmB is efficiently incorporated into snRNPs (Clelland 2009) and co-localizes with endogenous Sm proteins within the nucleus (Fig. 4A).

Two of these lines, mCherrySmBSHY03 and mCherrySmBSHY12, were used for FRAP analyses following transfection with a plasmid to reduce SMN levels or with control plasmids (targeting expression of PPIB or non-targeting). Transfected cells were identified by their expression of GFP. Using a texas red filter set to visualize mCherry, nuclear speckles were bleached using a fixed laser pulse of 1 second at 532 nm and short adaptive time-lapse sequences taken to determine the recovery kinetics (Fig. 4B,C). Comparison of these kinetics in SMN-depleted cells versus control cells revealed a significant decrease in the half-time of recovery of mCherry-SmB-tagged snRNPs to splicing speckles in cells with lowered levels of SMN (Fig 4D). The mobile fraction of mCherry-SmB-tagged snRNPs, around 40%, was unaltered by depletion of SMN. The immobile fraction of mCherry-SmB is larger than that seen for many non-snRNP splicing factors, in agreement with previous data (Sleeman 2007, Rino et al, 2007, Huranova et al, 2010). The nature of this immobile fraction is not known, but it is unlikely to represent snRNPs actively involved in pre-mRNA splicing as splicing occurs co-transcriptionally and not within speckles.

We have previously observed that the kinetics of exchange of photoactivatable GFP-SmB-containing snRNPs in Cajal bodies are best modeled using a two phase, rather than a one phase, exponential decay curve (Sleeman, 2007) with a slow moving and a rapidly moving pool of signal present. It is difficult to determine the nature of the rapidly exchanging pool. It may represent free SmB or low-affinity binding of a sub-set of assembled snRNPs. Alternatively, it may suggest that the FRAP recovery is diffusion-coupled (Sprague and McNally, 2005). Comparison of non-linear regression models using the extra sum-of-squares F test demonstrates that the recovery of mCherry-SmB to nuclear speckles also fits significantly better to a two-phase than to a one-phase recovery curve (Fig. 4E). It is possible that the faster-moving component (t1/2 ~0.5s) represents free mCherry-SmB. The core Sm proteins are added onto snRNAs in an early, cytoplasmic, stage of snRNP biogenesis with the Sm protein and tri-methylguanosine cap of the snRNA contributing to the nuclear import signal of the partially mature snRNP (Huber et al., 2002; Narayanan et al., 2004; Ospina et al., 2005). We would, therefore, not expect to find a significant amount of free mCherry-SmB in the nucleus. However, nuclear import of free Sm proteins has not been conclusively ruled out. In each of our experiments, both the t1/2 of this faster component, and the amount of the

signal recovering rapidly, remained constant while the t1/2 of the slower moving fraction decreased significantly (Fig. 4F). We can, therefore, be confident that the alterations in dynamics of mCherry-SmB observed represent alterations in the mobility of intact snRNPs, rather than an increase in any free mCherry-SmB present in the nucleus. Our analysis suggests that, although splicing speckle morphology is not grossly disrupted by the depletion of SMN, the dynamics of interaction of Sm-containing snRNPs with speckles are significantly altered. The increase in mobility of snRNPs within the nucleus is indicative of decreased affinity of binding to specific sites.

5) Both the major spliceosomal U1 snRNP and the minor splicosomal U11/U12 snRNP have altered mobility in cells depleted of SMN.

SmB is present in snRNPs from both the major (U1/U2) and minor (U11/U12) spliceosomes. Alterations in the repertoire of snRNPs have been implicated in the splicing defects seen in SMN-depleted HeLa cells and severe SMA mice with the suggestion that the levels of minor snRNPs are preferentially affected by SMN depletion. However, these changes were different in different tissues and it is unclear whether all snRNPs or predominantly the minor U11/U12 snRNPs are affected. To address this, we extended our FRAP analyses to look independently at the dynamics of the U1 snRNP and the U11/U12 snRNP. SH-SY5Y cell lines constitutively expressing the U1snRNP-specific protein mCherry-U170K (Ellis et al., 2008, a gift from David Lleres and Angus Lamond, University of Dundee) were established and FRAP experiments performed as described above. A significant decrease in half-time of recovery of mCherry-U170K to speckles resulting from SMN depletion was also seen in these experiments (Fig. 5A, B). As with mCherry-SmB labeled snRNPs, the change only affected the slower moving fraction of the signal, with the relative amounts of slow and fast signal unaltered. This is indicative of increased mobility of mature, fully assembled U1 snRNPs. We next investigated the mobility of the U11/U12 snRNP-specific protein SNRNP35, which shows significant homology to U170K (Will et al., 1999, a gift from Prof. R. Lührmann, Max Plank Institute for Biophysical Chemistry). SH-SY5Y cell lines were established constitutively expressing mCherry-SNRNP35. The localization of mCherry-SNRNP35 was clearly nuclear with a slight accumulation in nuclear speckles (Fig. 4C) as previously reported for the equivalent protein in Arabidopsis (Lorkovic et al, 2005). FRAP experiments again demonstrated a significant reduction in the half-time of recovery of the slower moving fraction (Fig. 4D,E). Interestingly, the reduction seen for

the U11/U12-specific SNRNP35 protein was more dramatic than that seen for the U1snRNP-specific U170K protein, suggesting that both the abundance and the mobility of the minor snRNPs are preferentially affected by SMN depletion.

6) Increased snRNP mobility is seen in fibroblasts from a Spinal Muscular Atrophy Type 1 patient.

To ascertain the relevance of changes in intra-nuclear snRNP mobility to SMA, we investigated the mobility of mCherry-U170K in fibroblasts from an SMA type1 patient and his unaffected mother (Coriell cell repository lines GM03813 and GM03814 respectively). Again, no gross structural abnormalities of nuclear speckles were detected in the SMA patient fibroblasts (Fig. 6A,B). FRAP analyses of these fibroblasts expressing mCherry-U170K for 72 hours revealed a similar decrease in the half time of recovery of this protein to speckles as was observed in SH-SY5Y cells depleted of SMN experimentally (Fig. 5A,B). This clearly demonstrates that defects in splicing snRNP mobility are associated with lowered levels of SMN in patients as well as in our cell culture models of SMA.

7) The alteration in splicing snRNP dynamics is a direct consequence of defective snRNP biogenesis in SMN-depleted cells.

Splicing defects have been reported in several models of SMA including SMN-depleted cells, while early studies of SMN function also suggested that it may have an additional direct role in splicing (Pellizzoni et al., 1998). Since increased mobility of splicing factors can be caused by inhibition of transcription or splicing (Kruhlak et al., 2000; Phair and Misteli, 2000; Rino et al., 2007), it was important to determine whether the alteration of snRNP dynamics caused by SMN depletion occurs as a result of defects in splicing or is a potential mechanism for the defects. To address this, we made a detailed analysis of the kinetic changes seen in cells treated to inhibit different stages of mRNA production. Cell lines stably expressing mCherry-SmB were treated with 5,6-dichloro-1-ß-D-ribobenzimidazole (DRB) to inhibit transcription, spliceostatin A (SSA) (Kaida et al., 2007, a gift from M. Yoshida, RIKEN, Japan) to inhibit pre-mRNA splicing directly and leptomycin B (LMB) (Fornerod et al., 1997) to inhibit the export of nascent snRNAs and, hence, to indirectly inhibit snRNP assembly. In agreement with previous reports studying a number of different splicing factors (Rino et al., 2007), DRB treatment resulted in significantly faster kinetics of exchange of snRNPs within speckles, again affecting preferentially the slower moving fraction (Fig. 7). However, in contrast to our

results seen in SMN-depleted cells, DRB treatment also resulted in a significant increase in the mobile fraction of rapidly moving signal and in noticeably altered speckle morphology (Fig. 7). Direct inhibition of splicing with SSA resulted in alterations in speckle morphology indistinguishable from those produced by inhibition of transcription by DRB (Fig. 7). However, this was associated with an increase in the mobile fraction of the slower moving component but no significant alteration in either t1/2. We have previously reported that inhibition of snRNP assembly with LMB for three hours does not affect the interaction of transiently expressed PA-GFP-SmB-tagged-snRNPs with speckles (Sleeman, 2007). This remains the case in cells stably expressing mCherry-SmB. However, treatment with LMB for 16 hours or more can successfully replicate the changes in dynamics seen in SMN-depleted cells (Fig. 7) with no discernable alterations to speckle morphology. This in-vitro modelling indicates that the changes in snRNP dynamics seen in SMN-depleted cells do not result from indirect or direct inhibition of pre-mRNA splicing, but are a direct consequence of inefficient splicing snRNP maturation (Fig. 8).

DISCUSSION

SMN depletion does not alter splicing speckle morphology but leads to significant changes in splicing snRNP dynamics.

The role of SMN in splicing snRNP biogenesis is well established. Despite evidence that SMN depletion has a profound effect on the formation of new snRNPs (reviewed in Chari et al., 2009), no obvious alteration in speckle morphology is seen in SMN-deficient cells using antibodies to snRNP proteins, snRNAs or non-snRNP splicing factors (Figs. 3 and 6). Analysis of the exchange of snRNPs within splicing speckles, however, reveals a significant increase in the intra-nuclear mobility of mature snRNPs in SMN-depleted cells and in cells from an SMA patient. Increased mobility of snRNPs is indicative of their reduced interaction with binding sites within the nucleus. This observation emphasises the importance of examining the flux of factors, rather than just their steady state localization, when investigating dynamic nuclear compartments.

Dynamics of both the major spliceosomal U1 snRNP and the minor spliceosomal U11/U12 snRNP are affected by SMN depletion

While there are now a number of reports of splicing defects associated with lowered levels of SMN, including both changes to alternative splicing and inaccurate or defective splicing, the mechanism for these defects is unclear. Alterations in the repertoire of snRNPs have been noted in HeLa cells, MN1 cells and mouse models of SMA (Gabanella et al., 2007; Zhang et al., 2008) with the minor U11 and U12 snRNPs preferentially affected. However, splicing defects seen in mouse models (Baumer et al., 2009; Zhang et al., 2008) and higher rates of errors in splice site pairing seen in SMA patient fibroblasts (Fox-Walsh and Hertel, 2009) do not appear to preferentially affect transcripts spliced by the minor spliceosome. Other studies have not detected significant alterations in the amounts of steady-state snRNPs (Boulisfane et al., 2011; Girard et al., 2006; Lemm et al., 2006). Defects in assembly of the minor spliceosome tri-snRNP have been implicated in altered splicing of minor introns in SMA patient lymphoblasts (Boulisfane et al., 2011). We have identified alterations in the dynamics of bulk splicing snRNPs using mCherry-tagged core Sm proteins in cells expressing shRNAs targeting SMN. More detailed analyses revealed that these alterations affect both the major spliceosomal U1 snRNP (tagged with nCherry-U170K) and the minor spliceosomal U11/U12 snRNP (tagged with mCherry-SNRNP35). While the alterations in dynamics of mCherry-SmB-tagged

snRNPs were unlikely exclusively to reflect defects in the mobility of the minor spliceosomal snRNPs, present at 100 times lower amounts that the major snRNPs, the equivalent alterations seen using mCherry-U170K as a tag confirm that the major U1 snRNP, and not just the minor U11/U12 snRNP, shows increased mobility. The alteration in U11/U12 snRNP dynamics was, however, greater than that in U1 snRNP dynamics, in broad agreement with the body of literature demonstrating more profound changes in the amounts of minor spliceosomal snRNPs in SMA models. Our data link SMN depletion to changes in the dynamic behaviour of snRNPs of the major and the minor spliceosomes.

Sensitivity to SMN-depletion varies in different cell types.

The SH-SY5Y neuroblastoma cell lines analysed in this study are viable for at least four days with levels of SMN, approximately 50% of wild-type, low enough to cause defects in snRNP mobility. However, we have so far been unable to establish SH-SY5Y cell lines with levels of SMN stably reduced by more than 10%. Experiments on HeLa cells (Zhang et al., 2008) demonstrated no loss of viability or changes in snRNP repertoire in cells expressing only ~20% of normal SMN levels while the reduction to ~5% required to see changes in splicing also resulted in cell death over 2-3 days. However, SMA mice (Zhang et al, 2008) survive with levels of SMN low enough to result in splicing defects and SMA patient fibroblasts are fully viable despite showing defects in snRNP mobility similar to those seen in SH-SY5Y cells with levels of SMN that are only achievable for short periods. Comparison of these data emphasise the different sensitivities of different cell types to the depletion of SMN. Since SMA preferentially affects spinal motor neurons, despite the need for snRNP assembly and accurate splicing in all cell types, this is highly relevant to the pathology of SMA.

Increased mobility of snRNPs suggests a mechanism for inefficient spliceosome formation resulting from defective snRNP biogenesis.

The mobility of factors within the nucleus occurs by anomalous diffusion, with reduced mobility resulting from interactions with specific binding sites. In the case of splicing snRNPs, the key interaction expected to retard their mobility is their incorporation into active spliceosomes (Rino et al., 2007). Increased mobility of splicing snRNPs in SMN-depleted cells is, therefore, indicative of reduced binding of snRNPs within active spliceosomes. Pre-mRNA splicing is a highly dynamic process, with spliceosome assembly in vivo proposed to occur by self-organization. Splice site selection is complex

and determined by the balance of many positive and negative regulators (reviewed in Wahl et al., 2009). However, in the major spliceosome, the binding of U1 snRNP to the 5' splice site is a key requirement for the formation of the spliceosomal E complex during the earliest stages of spliceosome assembly. The widespread defects in pre-mRNA splicing seen by Zhang et al appeared to preferentially involve genes with high numbers of introns and exons. They included not only altered selection of alternative splice sites but also defective splicing, suggesting a general lack of fidelity in the splicing process. To investigate the cause of such splicing defects, it is important to determine whether the changes in snRNP dynamics we see are a consequence of defective splicing resulting from SMN depletion by a mechanism unrelated to snRNP biogenesis or represent a potential link between defective snRNP biogenesis and altered splicing.

Our in vivo modelling using inhibitors of different stages of pre-mRNA processing was designed to address a specific question: do the changes in snRNP mobility seen result from splicing defects or are they a potential cause for them? The results clearly demonstrate that the changes seen in snRNP dynamics in SMN-depleted cells can only be replicated by reducing the snRNP assembly pathway. LMB is known to inhibit snRNP maturation at the point of snRNA export into the cytoplasm by binding directly to the export receptor CRM1 (Kudo et al, 1997). This step closely precedes the addition of Sm proteins to the snRNA, which is mediated by the SMN complex and impaired in SMN-depleted cells (Shpargel and Matera, 2005, Lemm et al, 2006). The inhibitor of transcriptional elongation, DRB, has traditionally been used as an indirect inhibitor of splicing. More recently SSA has been identified as a direct inhibitor of pre-mRNA splicing, believed to act via the formation of an arrested spliceosome containing U1 and U2 snRNPs (Roybal and Jurica, 2010) and impeding the transition from the A complex to the B complex. DRB, but not SSA, results in a significantly decreased half-time of recovery for the slower moving fraction of snRNPs, suggesting lower affinity interactions with spliceosomes in DRB treated cells. However, both inhibitors also result in alteration of speckle morphology and a significantly higher mobile fraction of snRNPs neither of which are seen in SMN-depleted cells. Mathematical modelling has previously demonstrated that decreasing the number of nucleoplasmic binding sites is sufficient to reproduce the effects on splicing factor kinetics and nuclear speckle morphology observed experimentally by inhibiting transcription using DRB, or splicing

using a dominant negative variant of the snRNP nuclear import adaptor snurportin1 (Rino et al., 2007). Decreased pre-mRNA transcription (caused by DRB) or the presence of stable arrested spliceosomes (caused by SSA) would both be predicted to reduce the number of nucleoplasmic splice sites available to bind snRNPs. Inhibition of splicing snRNP biogenesis using LMB, however, accurately replicates the changes seen in snRNP dynamics following SMN depletion (Fig. 7B,C). The half time of recovery of snRNPs is decreased indicating lowered affinity of interaction with spliceosomes while the mobile fraction remains the same suggesting that the number of binding events remains constant. In addition to implicating the alterations in snRNP mobility as a cause, rather than a consequence, of inefficient splicing, this provides a direct molecular link between the known function of SMN in cytoplasmic stages of snRNP assembly and defects in splicing observed in numerous models, without needing to invoke other, as yet unidentified, functions for SMN. While it is still unclear whether defective splicing of key motor neuron transcripts is at the root of the pathology of SMA, our data provide a mechanistic link between reduction of SMN, a key player in the generation of the cell's splicing machinery, and generalised defects in splicing.

There is increasing recognition that defects in RNA metabolism underly many human diseases, particularly motor neuron diseases (reviewed in Cooper et al., 2009; Lemmens et al., 2010). The finely balanced patterns of splicing seen in mammalian cells allow for rapid and sensitive adjustments to protein expression during the development and maintenance of complex tissues and organs. However, their intricate nature is susceptible to perturbation, with defects in proteins involved in pre-mRNA splicing pathways implicated in degenerative conditions such as ALS, and cancers in addition to SMA. Recent research into the degenerative eye condition, retinitis pigmentosa (RP), in which heterozygous mutations in splicing factors associated with the U4/U6.U5 tri-snRNP are implicated, has drawn striking parallels with SMA. Both SMA and RP appear to be systemic splicing diseases with cell type-specific symptoms (Linder et al., 2011; Tanackovic et al., 2011a; Tanackovic et al., 2011b). This implicates disrupted spliceosome assembly and dynamics as the cause of at least two degenerative conditions.

Materials and Methods

Cell Culture and Cell Lines

Cells were grown in Dulbecco's modified Eagle's medium (DMEM) supplemented with 10% fetal calf serum and 100 U/ml penicillin and streptomycin (Invitrogen). For immunofluorescence assays, cells were gown on coverslips (VWR). For live-cell microscopy, cells were grown on 40mm diameter coverslips (Intracel). Stable cell lines were established using G418 selection of SH-SY5Y cells following transfection with plasmids pmCherry-SmB (Clelland et al., 2009) and pmCherry-U170K (Ellis et al., 2008, a gift from D.Lléres and A.I.Lamond, University of Dundee) with Effectene transfection reagent (Qiagen) as described previously (Sleeman et al, 2001). snRNP35 (a gift from C. Will and R. Lührmann, Max Plank Institute for Biological Chemistry, Gottingen) was sub-cloned into mCherry-C1 (Clontech) by Dundee Cell Products, Dundee. Stable cell lines were established as above. SMA patient and control fibroblasts were lines GM03813 and GM03814 respectively from the Coriell Cell Repository. For analysis of the effects of inhibitors of pre-mRNA processing, cells were incubated for 5 hours with 20µg/ml DRB (Sigma), 16 hours with 100ng/ml SSA (a gift from M. Yoshida, RIKEN, Japan), 3hrs, 6hrs or 16 hrs with 50ng/ml LMB (LC labs).

RNAi Assays

ON-TARGET plus siRNA duplexes (Dharmacon) were introduced into HeLa cells and SH-SY5Y cells using RNAiFect (Qiagen) according to the manufacturer's instructions. For shRNA expression, targeting sequences were cloned into pSuperGFP (oligoengine) according to the manufacturer's instruction and the resulting plasmids transfected into cells. Sequences used were: Lamin A/C: GGUGGUGACGAUCUGGGCU, non-targeting (luciferase): UAAGGCUAUGAAGAGAUAC; PPIB: GGAAAGACUGUUCCAAAAA; SMN 01: CAGUGGAAAGUUGGGGACA; SMN 05: UAUAUGGGUUUCAGACAAA.

Lamin A/C was used as a positive control in immunofluorescence assays and PPIB in western blot assays due to the differences in performance of antibodies to the two proteins in the different assays.

Cell fixation, immuno-staining and microscopy

HeLa cells grown on glass coverslips were fixed for 10 min at room temperature with

3.7% paraformaldehyde in PHEM buffer (60 mM PIPES, 25 mM HEPES, 10 mM EGTA, 2 mM MgCl2 [pH 6.9]). Immunostaining was carried out as described previously (Sleeman et al., 2003). Cells were mounted in Prolong Gold medium (Invitrogen). Antibodies used were mouse mAbs MANSMA1 anti-SMN (Young et al., 2000) (dilution 1:10), SC-35 (Sigma) (dilution 1:2000), Y12 anti-Sm (Abcam) (dilution 1:100), anti-TMG (Calbiochem, dilution 1:15) and rabbit 856 anti-U1A (Kambach and Mattaj, 1992) (dilution 1:500). Secondary antibodies were FITC- and TRITC-conjugated goat anti-mouse and goat anti-rabbit IgG (Jackson ImmunoResearch Laboratories) (dilution 1:250). Immunostained specimens were examined and recorded using a DeltaVision Spectris Deconvolution microscope with an Olympus 100X, 1.35NA objective and a Coolsnap HQ camera (Photometrics). Optical sections separated by 200 nm were collected using a binning of 2x2. Images were restored using an iterative deconvolution algorithm using a calculated point-spread function (Volocity, Perkin Elmer). Images in figures 1, 2 and 3 are maximum intensity projections of z-stacks covering the entire depth of the cells.

Quantitation of fluorescence signals

Quantitation of the proportion of SMN signal in transfected and untransfected cells and nuclei was carried out using an intensity threshold on stacks of deconvolved z-sections. A segmentation algorithm was used to find 'objects' by applying a global threshold to each stack of z-sections. Objects were defined as sets of contiguous pixels above the specified threshold. To identify transfected cells, GFP signal was used to identify 'objects', to identify untransfected cells, SMN signal was used. To identify nuclei, DAPI staining was used for 'object' identification and the transfected cells identified manually by reference to the overlaid GFP signal. In each case, the total SMN signal contained in each cell or nucleus was normalized to the total SMN fluorescence of the brightest cell or nucleus in the field of view following a correction to allow for background fluorescence within the sample.

Preparation of cell lysates and immunoblotting

Lysates were prepared as described previously (Sleeman et al., 2003), electrophoresed on a 10% SDS polyacrylamide gel (Invitrogen) and transferred to nitro-cellulose membranes (Hybond C+, GE Healthcare) for immunoblotting. Antibodies used were

rabbit anti-SMN (Santa Cruz, 1:500) and mouse anti-α-tubulin (Sigma, 1:1000). Secondary antibodies were HRP-conjugated anti-mouse or anti-rabbit (Pierce, 1:20000). Detection was carried out with ECL Plus Western Blotting Detection System (GE Healthcare) imaged using a Fujifilm LAS-3000 imaging system. Stripping of blots for re-probing with anti-tubulin antibodies was carried out by incubating the blots at 50°C for 30 minutes with 2% SDS, 100mM β–mercaptoethanol and 62.5 mM tris pH6.8.

Live Cell Microscopy and FRAP Analyses

Cells were grown on 40mm diameter glass coverslips and transfected with pSuper-GFP plamids 48hrs or 72hrs before analysis. The coverslips were transferred to an open chamber (Zeiss) within an environmental incubator (Solent Scientific) on an Olympus DeltaVision RT microscope (Applied Precision) with a Quantifiable Laser Module including a 20mW 532nm laser and maintained at 37°C with 5% CO_2. Transfected cells expressing GFP were identified using FITC filters. Nuclear speckles within selected cells were bleached using a 1s 532nm pulse at 100% laser power focused to a diffraction-limited spot of approximately 0.5 μm. The duration of bleaching achieved a reduction of fluorescence in the region of interest of approximately 60%. A single z-section of each cell was imaged using a texas red filter at 3 timepoints before the laser pulse and an adaptive time course of 32 timepoints after the laser pulse. For single-phase recovery analyses, images were normalized for mean intensity and models generated using the method of Axelrod (Axelrod et al., 1976) as implemented within SoftWoRx software. For comparison of one-phase and two-phase recovery, the intensities of the region of interest, corrected for photo-bleaching, were normalized against the initial pre-bleach fluorescence and plotted against time. One- and two-phase exponential association curves were fitted to each data set and an extra sum-of-squares F test performed to determine which model gave the better fit (GraphPad Prism). In all cases, the two-phase curve gave the better fit ($P<0.0001$). Equations used were as follows:

$$Y=Ymax1 \times (1-\exp(-K1 \times X)) + Ymax2 \times (1-\exp(-K2 \times X))$$

$$Y=Ymax \times (1-\exp(-K \times X))$$

Half-times of recovery and mobile fractions were compared using a one-way ANOVA test with Tukey-Kramer post-test.

Acknowledgements

The authors would like to thank M. Yoshida (Riken, Japan) for providing spliceostatin A; D. Lleres and A.I.Lamond (University of Dundee, UK) for the plasmid to express mCherry-U170K; C. Will and R. Lührmann (Max Plank Institute for Biological Chemistry, Gottingen for the cDNA for SNRNP35; G.Morris (RJAH Orthopaedic Hospital, Oswestry, UK) for anti-SMN antibodies; L.Trinkle-Mulcahy (University of Ottawa, Canada) for helpful discussions and Prof R. Elliot (University of St Andrews, UK) for critical reading of the manuscript. This work was funded by the Wellcome Trust and the Royal Society. The authors declare no conflicts of interest.

REFERENCES

Axelrod, D., Koppel, D. E., Schlessinger, J., Elson, E. and Webb, W. W. (1976). Mobility measurement by analysis of fluorescence photobleaching recovery kinetics. *Biophys J* **16**, 1055-1069.

Battle, D. J., Kasim, M., Yong, J., Lotti, F., Lau, C. K., Mouaikel, J., Zhang, Z., Han, K., Wan, L. and Dreyfuss, G. (2006). The SMN complex: an assembly machine for RNPs. *Cold Spring Harb Symp Quant Biol* **71**, 313-320.

Baumer, D., Lee, S., Nicholson, G., Davies, J. L., Parkinson, N. J., Murray, L. M., Gillingwater, T. H., Ansorge, O., Davies, K. E. and Talbot, K. (2009). Alternative splicing events are a late feature of pathology in a mouse model of spinal muscular atrophy. *PLoS Genet* **5**, e1000773.

Boulisfane, N., Choleza, M., Rage, F., Neel, H., Soret, J. and Bordonne, R. (2011). Impaired minor tri-snRNP assembly generates differential splicing defects of U12-type introns in lymphoblasts derived from a type I SMA patient. *Hum Mol Genet* **20**, 641-648.

Campion, Y., Neel, H., Gostan, T., Soret, J. and Bordonne, R. (2010). Specific splicing defects in S. pombe carrying a degron allele of the Survival of Motor Neuron gene. *Embo J* **29**, 1817-1829.

Carvalho, T., Almeida, F., Calapez, A., Lafarga, M., Berciano, M. T. and Carmo-Fonseca, M. (1999). The spinal muscular atrophy disease gene product, SMN: A link between snRNP biogenesis and the Cajal (coiled) body. *J Cell Biol* **147**, 715-728.

Chari, A., Paknia, E. and Fischer, U. (2009). The role of RNP biogenesis in spinal muscular atrophy. *Curr Opin Cell Biol* **21**, 387-393.

Cioce, M. and Lamond, A. I. (2005). Cajal bodies: a long history of discovery. *Annu Rev Cell Dev Biol* **21**, 105-131.

Clelland, A. K., Kinnear, N. P., Oram, L., Burza, J. and Sleeman, J. E. (2009). The SMN protein is a key regulator of nuclear architecture in differentiating neuroblastoma cells. *Traffic* **10**, 1585-1598.

Cooper, T. A., Wan, L. and Dreyfuss, G. (2009). RNA and disease. *Cell* **136**, 777-793.

Coovert, D. D., Le, T. T., McAndrew, P. E., Strasswimmer, J., Crawford, T. O., Mendell, J. R., Coulson, S. E., Androphy, E. J., Prior, T. W. and Burghes, A. H. (1997). The survival motor neuron protein in spinal muscular atrophy. *Hum Mol Genet* **6**, 1205-1214.

Ellis, J. D., Lleres, D., Denegri, M., Lamond, A. I. and Caceres, J. F. (2008). Spatial mapping of splicing factor complexes involved in exon and intron definition. *J Cell Biol* **181**, 921-934.

Fornerod, M., Ohno, M., Yoshida, M. and Mattaj, I. W. (1997). CRM1 is an export receptor for leucine-rich nuclear export signals. *Cell* **90**, 1051-1060.

Fox-Walsh, K. L. and Hertel, K. J. (2009). Splice-site pairing is an intrinsically high fidelity process. *Proc Natl Acad Sci U S A* **106**, 1766-1771.

Gabanella, F., Butchbach, M. E., Saieva, L., Carissimi, C., Burghes, A. H. and Pellizzoni, L. (2007). Ribonucleoprotein assembly defects correlate with spinal muscular atrophy severity and preferentially affect a subset of spliceosomal snRNPs. *PLoS ONE* **2**, e921.

Girard, C., Neel, H., Bertrand, E. and Bordonne, R. (2006). Depletion of SMN by RNA interference in HeLa cells induces defects in Cajal body formation. *Nucleic Acids Res* **34**, 2925-2932.

Gonsalvez, G. B., Tian, L., Ospina, J. K., Boisvert, F. M., Lamond, A. I. and Matera, A. G. (2007). Two distinct arginine methyltransferases are required for biogenesis of Sm-class ribonucleoproteins. *J Cell Biol* **178**, 733-740.

Huber, J., Dickmanns, A. and Luhrmann, R. (2002). The importin-beta binding domain of snurportin1 is responsible for the Ran- and energy-independent nuclear import of spliceosomal U snRNPs in vitro. *J Cell Biol* **156**, 467-479.

Huranová, M., Ivani, I., Benda, A., Poser, I., Brody, Y., Hof, M., Shav-Tal, Y., Neugebauer, K.M., Stanek, D. (2010). The differential interaction of snRNPs with pre-mRNA reveals splicing kinetics in living cells. *J Cell Biol* 191, 75-86.

Iborra, F. J. and Cook, P. R. (2002). The interdependence of nuclear structure and function. *Curr Opin Cell Biol* **14**, 780-785.

Kaida, D., Motoyoshi, H., Tashiro, E., Nojima, T., Hagiwara, M., Ishigami, K., Watanabe, H., Kitahara, T., Yoshida, T., Nakajima, H. et al. (2007). Spliceostatin A targets SF3b and inhibits both splicing and nuclear retention of pre-mRNA. *Nat Chem Biol* **3**, 576-583.

Kambach, C. and Mattaj, I. W. (1992). Intracellular distribution of the U1A protein depends on active transport and nuclear binding to U1 snRNA. *J Cell Biol* **118**, 11-21.

Kambach, C., Walke, S., Young, R., Avis, J. M., de la Fortelle, E., Raker, V. A., Luhrmann, R., Li, J. and Nagai, K. (1999). Crystal structures of two Sm protein

complexes and their implications for the assembly of the spliceosomal snRNPs. *Cell* **96**, 375-387.

Kruhlak, M. J., Lever, M. A., Fischle, W., Verdin, E., Bazett-Jones, D. P. and Hendzel, M. J. (2000). Reduced mobility of the alternate splicing factor (ASF) through the nucleoplasm and steady state speckle compartments. *J Cell Biol* **150**, 41-51.

Kudo, N., Wolff, B., Sekimoto, T., Schreiner, E.P., Yoneda, Y., Yanagida, M., Horinouchi, S., Yoshida, M. (1998) Leptomycin B inhibition of signal-mediated nuclear export by direct binding to CRM1. *Exp Cell Res* 242, 540-547.

Lefebvre, S., Burlet, P., Liu, Q., Bertrandy, S., Clermont, O., Munnich, A., Dreyfuss, G. and Melki, J. (1997). Correlation between severity and SMN protein level in spinal muscular atrophy. *Nat Genet* **16**, 265-269.

Lemm, I., Girard, C., Kuhn, A. N., Watkins, N. J., Schneider, M., Bordonne, R. and Luhrmann, R. (2006). Ongoing U snRNP biogenesis is required for the integrity of Cajal bodies. *Mol Biol Cell* **17**, 3221-3231.

Lemmens, R., Moore, M. J., Al-Chalabi, A., Brown, R. H., Jr. and Robberecht, W. (2010). RNA metabolism and the pathogenesis of motor neuron diseases. *Trends Neurosci* **33**, 249-258.

Linder, B., Dill, H., Hirmer, A., Brocher, J., Lee, G. P., Mathavan, S., Bolz, H. J., Winkler, C., Laggerbauer, B. and Fischer, U. (2011). Systemic splicing factor deficiency causes tissue-specific defects: a zebrafish model for retinitis pigmentosa. *Hum Mol Genet* **20**, 368-377.

Liu, Q. and Dreyfuss, G. (1996). A Novel Nuclear-Structure Containing the Survival Of Motor-Neurons Protein. *Embo Journal* **15**, 3555-3565.

Lorković, Z.J., Lehner, R., Forstner, R. and Barta, A. (2005). Evolutionary conservation of minor U12-type spliceosome between plants and humans. *RNA* **11**,1095–1107.

Misteli, T. (2001a). The concept of self-organization in cellular architecture. *J Cell Biol* **155**, 181-185.

Misteli, T. (2001b). Protein dynamics: implications for nuclear architecture and gene expression. *Science* **291**, 843-847.

Misteli, T. (2010). Higher-order genome organization in human disease. *Cold Spring Harb Perspect Biol* **2**, a000794.

Narayanan, U., Achsel, T., Luhrmann, R. and Matera, A. G. (2004). Coupled in vitro import of U snRNPs and SMN, the spinal muscular atrophy protein. *Mol Cell* **16**, 223-234.

Ospina, J. K., Gonsalvez, G. B., Bednenko, J., Darzynkiewicz, E., Gerace, L. and Matera, A. G. (2005). Cross-talk between snurportin1 subdomains. *Mol Biol Cell* **16**, 4660-4671.

Patel, S. B. and Bellini, M. (2008). The assembly of a spliceosomal small nuclear ribonucleoprotein particle. *Nucleic Acids Res* **36**, 6482-6493.

Pellizzoni, L. (2007). Chaperoning ribonucleoprotein biogenesis in health and disease. *EMBO Rep* **8**, 340-345.

Pellizzoni, L., Kataoka, N., Charroux, B. and Dreyfuss, G. (1998). A novel function for SMN, the spinal muscular atrophy disease gene product, in pre-mRNA splicing. *Cell* **95**, 615-624.

Phair, R. D. and Misteli, T. (2000). High mobility of proteins in the mammalian cell nucleus. *Nature* **404**, 604-609.

Rino, J. and Carmo-Fonseca, M. (2009). The spliceosome: a self-organized macromolecular machine in the nucleus? *Trends Cell Biol* **19**, 375-384.

Rino, J., Carvalho, T., Braga, J., Desterro, J. M., Luhrmann, R. and Carmo-Fonseca, M. (2007). A stochastic view of spliceosome assembly and recycling in the nucleus. *PLoS Comput Biol* **3**, 2019-2031.

Roybal, G. A. and Jurica, M. S. (2010). Spliceostatin A inhibits spliceosome assembly subsequent to prespliceosome formation. *Nucleic Acids Res* **38**, 6664-6672.

Schaffert, N., Hossbach, M., Heintzmann, R., Achsel, T. and Luhrmann, R. (2004). RNAi knockdown of hPrp31 leads to an accumulation of U4/U6 di-snRNPs in Cajal bodies. *Embo J* **23**, 3000-3009.

Shpargel, K. B. and Matera, A. G. (2005). Gemin proteins are required for efficient assembly of Sm-class ribonucleoproteins. *Proc Natl Acad Sci U S A* **102**, 17372-17377.

Sleeman, J. (2007). A regulatory role for CRM1 in the multi-directional trafficking of splicing snRNPs in the mammalian nucleus. *J Cell Sci* **120**, 1540-1550.

Sleeman, J. E. and Lamond, A. I. (1999). Newly assembled snRNPs associate with coiled bodies before speckles, suggesting a nuclear snRNP maturation pathway. *Curr Biol* **9**, 1065-1074.

Sleeman, J. E., Trinkle-Mulcahy, L., Prescott, A. R., Ogg, S. C. and Lamond, A. I. (2003). Cajal body proteins SMN and Coilin show differential dynamic behaviour in vivo. *J Cell Sci* **116**, 2039-2050.

Spector, D. L. and Lamond, A. I. (2011). Nuclear speckles. *Cold Spring Harb Perspect Biol* **3**.

Sprague, B. L. and McNally, J. G. (2005). FRAP analysis of binding: proper and fitting. *Trends Cell Biol* **15**, 84-91.

Stanek, D., Rader, S. D., Klingauf, M. and Neugebauer, K. M. (2003). Targeting of U4/U6 small nuclear RNP assembly factor SART3/p110 to Cajal bodies. *J Cell Biol* **160**, 505-516.

Stanek, D., Pridalova-Hnilicova, J., Novotny, I., Huranova, M., Blazikova, M., Wen, X., Sapra, A. K. and Neugebauer, K. M. (2008). Spliceosomal small nuclear ribonucleoprotein particles repeatedly cycle through Cajal bodies. *Mol Biol Cell* **19**, 2534-2543.

Stark, H., Dube, P., Luhrmann, R. and Kastner, B. (2001). Arrangement of RNA and proteins in the spliceosomal U1 small nuclear ribonucleoprotein particle. *Nature* **409**, 539-542.

Tanackovic, G., Ransijn, A., Ayuso, C., Harper, S., Berson, E. L. and Rivolta, C. (2011a). A Missense Mutation in PRPF6 Causes Impairment of pre-mRNA Splicing and Autosomal-Dominant Retinitis Pigmentosa. *Am J Hum Genet* **88**, 643-649.

Tanackovic, G., Ransijn, A., Thibault, P., Abou Elela, S., Klinck, R., Berson, E. L., Chabot, B. and Rivolta, C. (2011b). PRPF mutations are associated with generalized defects in spliceosome formation and pre-mRNA splicing in patients with retinitis pigmentosa. *Hum Mol Genet* **20**, 2116-2130.

Tarn, W. Y. and Steitz, J. A. (1996). A novel spliceosome containing U11, U12, and U5 snRNPs excises a minor class (AT-AC) intron in vitro. *Cell* **84**, 801-811.

Wahl, M. C., Will, C. L. and Luhrmann, R. (2009). The spliceosome: design principles of a dynamic RNP machine. *Cell* **136**, 701-718.

Wan, L., Battle, D. J., Yong, J., Gubitz, A. K., Kolb, S. J., Wang, J. and Dreyfuss, G. (2005). The survival of motor neurons protein determines the capacity for snRNP assembly: biochemical deficiency in spinal muscular atrophy. *Mol Cell Biol* **25**, 5543-5551.

Will, C. L. and Luhrmann, R. (2001). Spliceosomal UsnRNP biogenesis, structure and function. *Curr Opin Cell Biol* **13**, 290-301.

Will, C.L., Schneider, C., Reed, R.,and Lührmann, R. (1999), Identification of both shared and distinct proteins in the major and minor spliceosomes. *Science* 284, 2003-2005.

Young, P. J., Le, T. T., thi Man, N., Burghes, A. H. and Morris, G. E. (2000). The relationship between SMN, the spinal muscular atrophy protein, and nuclear coiled bodies in differentiated tissues and cultured cells. *Exp Cell Res* **256**, 365-374.

Zhang, Z., Lotti, F., Dittmar, K., Younis, I., Wan, L., Kasim, M. and Dreyfuss, G. (2008). SMN deficiency causes tissue-specific perturbations in the repertoire of snRNAs and widespread defects in splicing. *Cell* **133**, 585-600.

Figures and Legends

Figure1

SMN can be effectively reduced by RNAi in HeLa and SH-SY5Y cells

A) Immunofluorescent detection of SMN (green, left hand panels) in HeLa cells transiently transfected with siRNA duplexes shows lowered staining and loss of nuclear gems (arrows in control panels i and ii) in cells transfected with two independent duplexes targeting SMN (panels iii and iv). Right hand panels (DAPI) show the positions of the nuclei. Bar=10μm. B). The number of nuclear gems per cell is dramatically reduced by siRNA duplexes in HeLa cells. Data represented as mean+/- SEM, n=80 cells per duplex pooled from two independent experiments. C) Western blot analysis of SH-SY5Y cells transfected with siRNA duplexes targeting SMN for 24 or 48hrs show a strong reduction in SMN protein compared to negative control non-targeting duplexes and positive control duplexes targeting PPIB. Anti-tubulin confirms even loading of samples. Lanes containing additional positive controls have been cut from the blot. D) Quantitation of western blots, normalized to tubulin signal, reveals a reduction to 48% of normal after 24 hours (mean of two independent experiments, data represented as mean+/- SEM) and to 32% of normal after 48hrs.

Figure 2

SMN reduction can be achieved using expression of shRNAs

Immunodetection of SMN (left hand panels and red signal in right hand panels) in cells transfected with plasmids to express shRNAs targeting SMN (A, B and C) or a positive control targeting PPIB (D). The inclusion of a GFP expression cassette on the plasmid allows unequivocal identification of transfected cells (green signal in right hand panel and arrows). Expression of shRNAs targeting SMN for 24hrs does not result in an appreciable decrease in SMN protein (A, arrowhead shows an SMN-positive nuclear gem), while 48hrs or 72hrs of expression results in loss of SMN from the nucleus and cytoplasm (B and C). Cells expressing shRNAs to PPIB show strong SMN expression at all three time points (D and other data not shown). Bar=10μm. E) Quantitation of anti-SMN fluorescence signal in transfected and untransfected cells and nuclei demonstrate reduction of SMN to 46% of control in whole cells and to 56% of control in nuclei.

Measurements were made from deconvolved z-stacks of a total of 40 cells, data represented as mean+/- SEM.

Figure 3

Reduction of SMN does not disrupt the structure of splicing speckles.

SMN-depleted SH-SY5Y cells (identified by GFP expression, green in lower panels) show normal speckled distribution of the SR splicing factor, SC-35 (A), the core snRNP Sm proteins (B), the U1 snRNP-specific protein U1A (C) and snRNAs detected using antibodies to their tri-methyl guanosine cap structure (D). Cytoplasmic accumulations of snRNAs are also readily detected in both SMN-depleted and control cells (arrowheads in D). Bar=10μm.

Figure 4

SMN depletion increases the mobility of mCherry-SmB-tagged splicing snRNPs, preferentially affecting a slow-moving fraction.

A) Stably expressed mCherry-SmB (i, red in iii) co-localises with endogenous Sm proteins (ii, green in iii) in SH-SY5Y cells. The signal is predominantly within the nucleus, identified by DAPI staining (blue) in iii) with clear accumulation seen in splicing speckles (arrows in C). Bar=10μm. B) Representative images of a FRAP experiment in cell line mCherrySmBSHY12. The magenta circle marks the bleach region with the pseudocolour spectrum showing the highest intensity pixels in red and the lowest in blue. Images show the cell before bleaching, immediately after bleaching and at the end of the recovery time-course when partial recovery of fluorescence has occurred. Bar=10μm. C) Recovery curves for cells transfected with control plasmids (black) or a plasmid expressing shRNA sequence SMN01 to deplete SMN (red). Mean +/- SEM from 30 FRAP time-courses for each condition, pooled from two independent experiments. D) The observed half-time of recovery of mCherrySmB to speckles is significantly reduced in cells with depleted SMN compared to those transfected with negative control plasmids (mCherrySmBSHY12 48 hours ($n=38$, $P<0.001$) and mCherrySmBSHY03 48 hours ($n=27$, $P<0.01$)) or positive control plasmids targeting PPIB (mCherrySmBSHY12 72 hours ($n=29$, $P<0.001$)). Although the half-life mCherrySmB in control cells of line mCherrySmBSHY03 is longer than that seen in line mCherrySmBSHY12, a similar decrease is seen following SMN reduction. The mobile

fraction of mCherrySmB is unaltered by SMN depletion in either cell line. All data represented as mean+/- SEM. E) Comparison of one-phase (dotted line) and two-phase (solid line) recovery models of FRAP data sets reveal a significantly better fit using a two-phase model ($P<0.0001$). Example data sets shown are of line mCherrySmBSHY12 transfected for 48hrs, also included in figure 4C. F) Detailed analysis of the recovery kinetics from mCherrySmBSHY12 reveals that the decrease in the overall half-time of recovery reflects increased mobility (decrease in t1/2) of a slower moving fraction of mCherrySmB, with a faster moving fraction unchanged by SMN-depletion. Data represented as mean +/- SEM, n=38.

Figure 5

SMN depletion increases the mobility of the major spliceosomal U1 snRNP and the minor spliceosomal U11/12 snRNP.

A) Representative images of a FRAP experiment in cell line mCherryU170KSHY05. The magenta circle marks the bleach region with the pseudocolour spectrum showing the highest intensity pixels in red and the lowest in blue. Images show the cell before bleaching, immediately after bleaching and at the end of the recovery time-course. Bar=10μm. B) Analysis of the FRAP kinetics of mCherry-U170K reveals an increase in the mobility of the slower-moving fraction of signal. Data represented as mean +/- SEM, n=82, pooled data from two independent experiments. C) Deconvolved images of mCherry-SNRNP35 (red) shows nuclear localization with a slight accumulation in nuclear speckles (arrows) detected with anti-Sm antbodies (green). D) Representative images of a FRAP experiment in cell line mCherrySNRNP35SHY02. Bar=10μm. E) Analysis of the FRAP kinetics of mCherry-SNRNP35 reveals an increase in the mobility of the slower-moving fraction of signal. Data represented as mean +/- SEM, n=37, pooled data from two independent experiments.

Figure 6

Fibroblasts from an SMA patient show an increase in snRNP mobility in the absence of disruption of splicing speckles.

Fibroblasts from an SMA patient (lower panels) show normal localisation of the SR splicing factor, SC-35 (A) and the core snRNP Sm proteins (B) to speckles (arrows)

when compared to fibroblasts from the patient's unaffected mother (upper panels). Bar=10μm. C) Analysis of the FRAP kinetics of mCherry-U170K transiently transfected into patient and control fibroblasts reveals an increase in the mobility of the slower-moving fraction of signal. Data represented as mean +/- SEM, n=58, pooled data from two independent experiments.

Figure 7

Inhibition of the snRNP processing pathway with leptomycin B accurately replicates the effects of SMN depletion

A) Representative images of live cells expressing mCherry-SmB treated with inhibitors of different stages of pre-mRNA processing. Inhibition of transcription (DRB) or splicing (SSA) results in abnormal splicing speckle morphology (arrows). Inhibition of snRNP assembly (LMB) has no detectable effect on the morphology of splicing speckles compared to the no drug control. B) FRAP recovery curves show altered dynamics in cells treated with DRB (blue), SSA (green) and LMB (red). The alteration in the curve obtained with LMB closely resembles that caused by SMN depletion (figure 4). Data represented as mean +/- SEM. C) Inhibition of transcription (DRB, blue) causes a significant decrease in the t1/2 of the slower moving fraction of snRNPs, accompanied by an increase in the mobile fraction of the faster component (n=69). Inhibition of pre-mRNA splicing (SSA, green) does not show a significant alteration in either t1/2 but results in a significant increase in the mobile fraction of the faster signal (n=70). Inhibition of snRNP processing (LMB, red) shows a similar decrease in the slower t1/2 as is seen in SMN-depleted cells, with unaltered mobile fractions (n=66).

Figure 8

Summary of the effects of inhibitors of different stages of pre-mRNA production on intra-nuclear snRNP mobility and splicing speckle structure

In control cells, snRNPs exchange continually between speckles (red) and active self-organized spliceosomes, denoted by the black arrow, leading to efficient splicing. The transcriptional inhibitor, DRB, reduces the number of splice sites present, resulting in a larger mobile fraction of snRNPs, faster return of snRNPs to speckles and abnormal speckle morphology. By arresting splicing with a stabilized A complex (pink star), SSA reduces the number of splice sites available for snRNP binding, again resulting in a

larger mobile fraction of snRNPs and abnormal speckle morphology. Reduction of the efficiency of snRNP assembly by LMB or reduction of SMN increases the rate of return of snRNPs to speckles, making them less available for spliceosome formation without affecting speckle morphology.

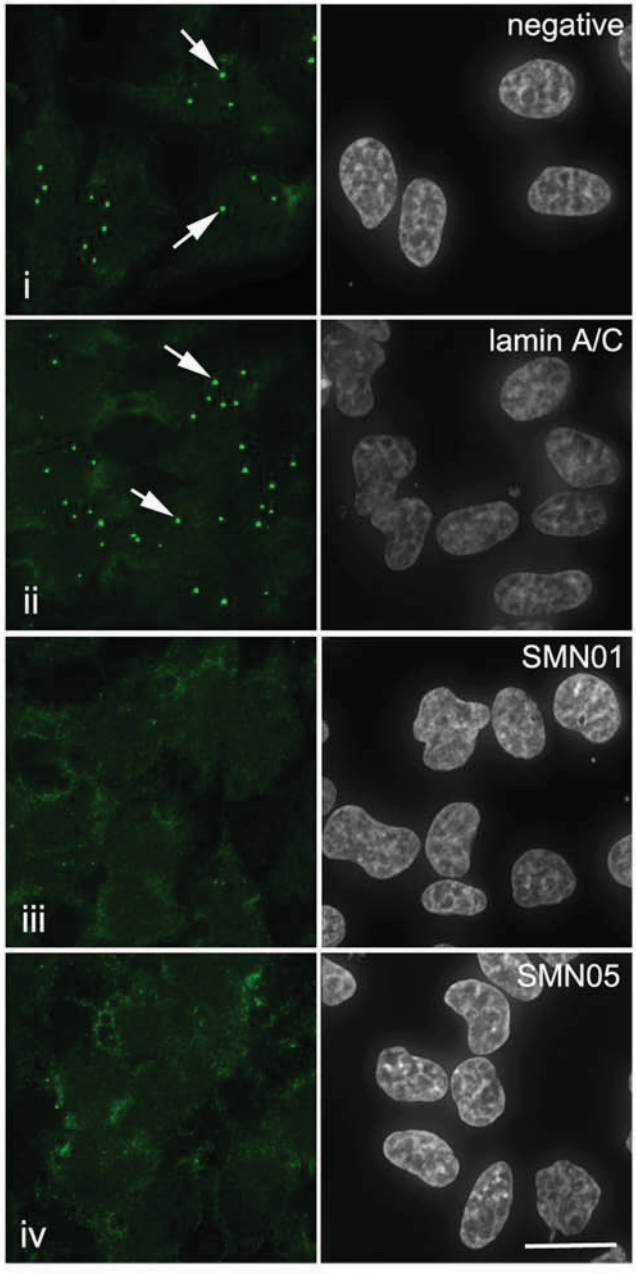

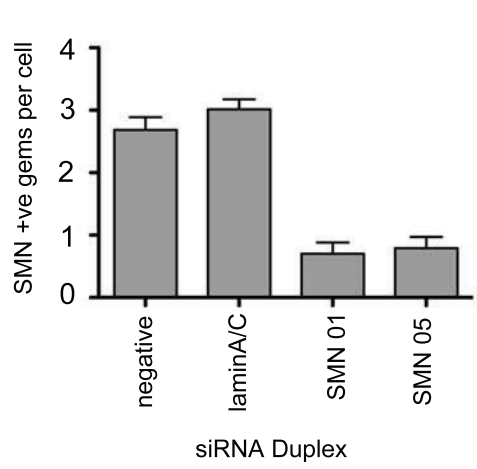

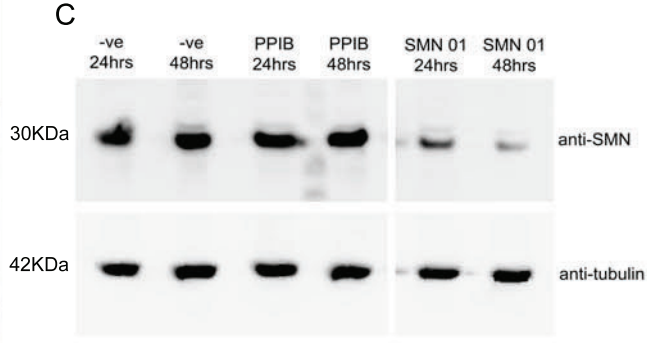

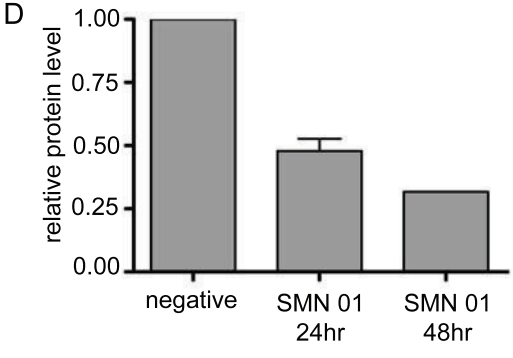

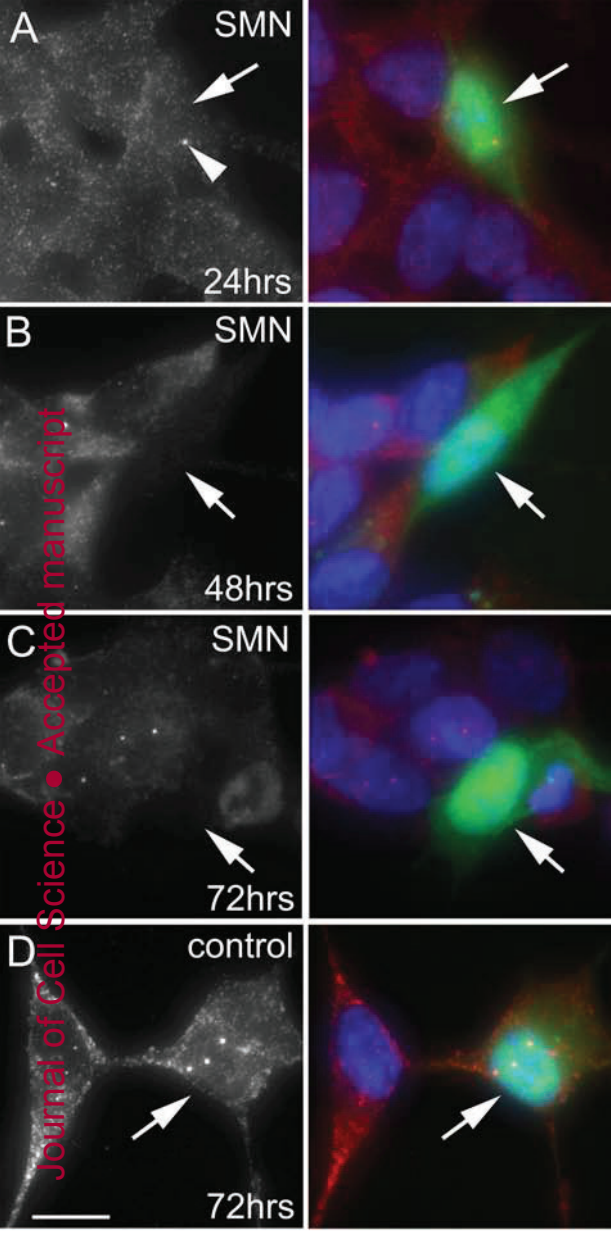

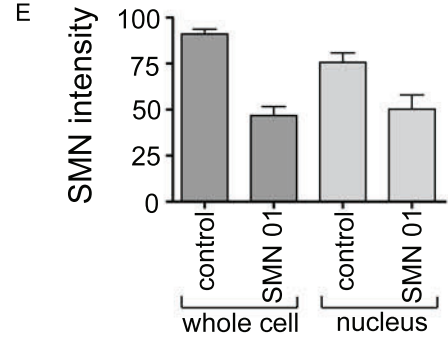

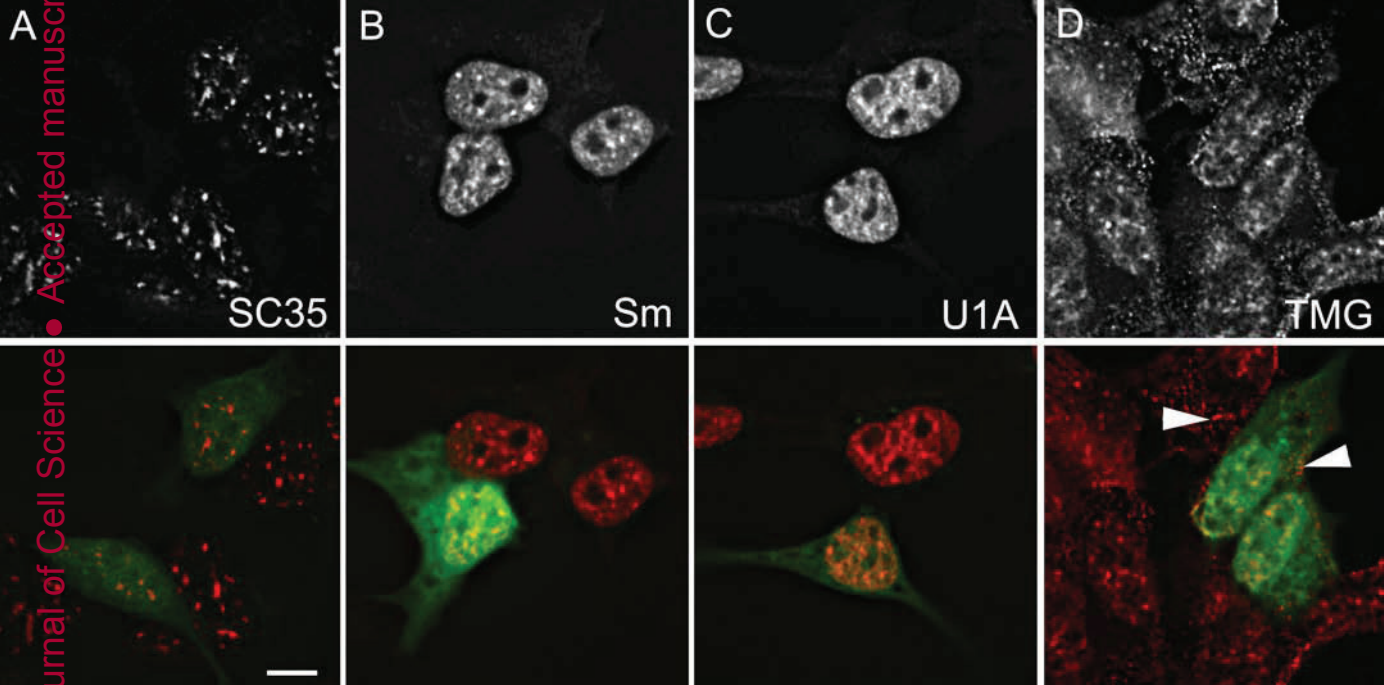

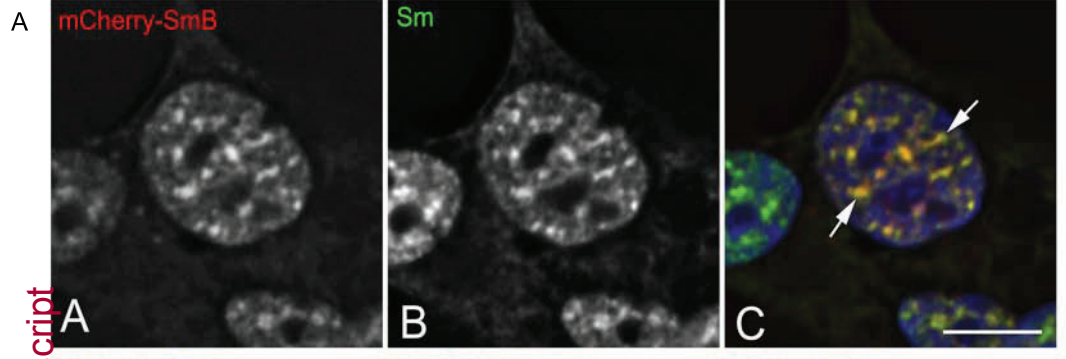

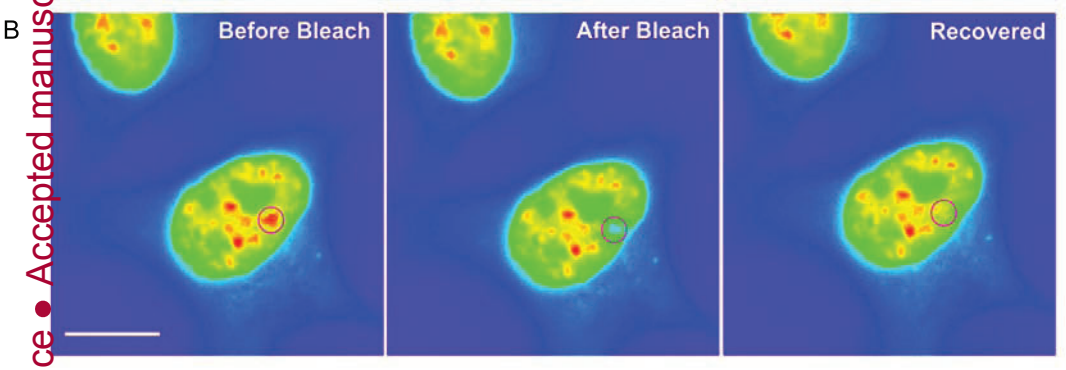

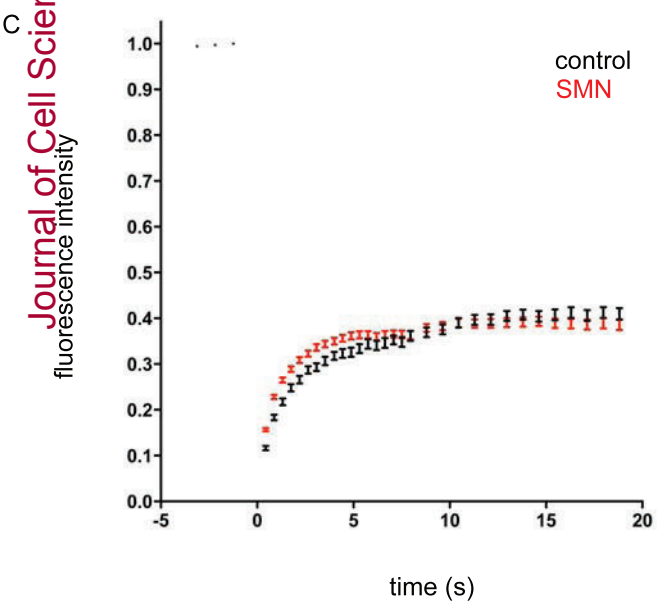

D

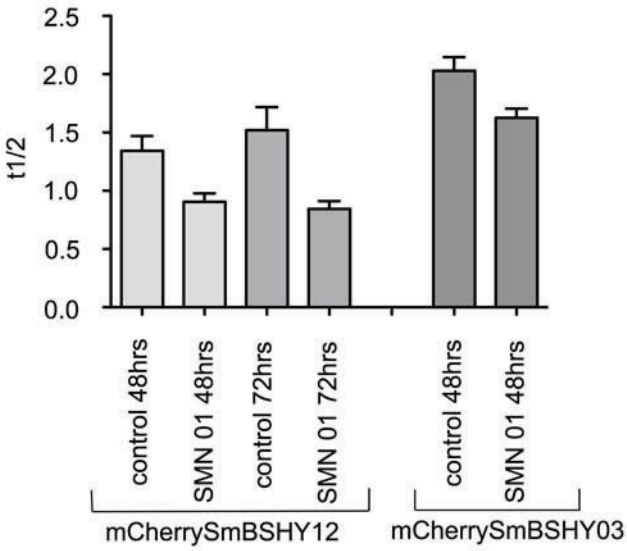

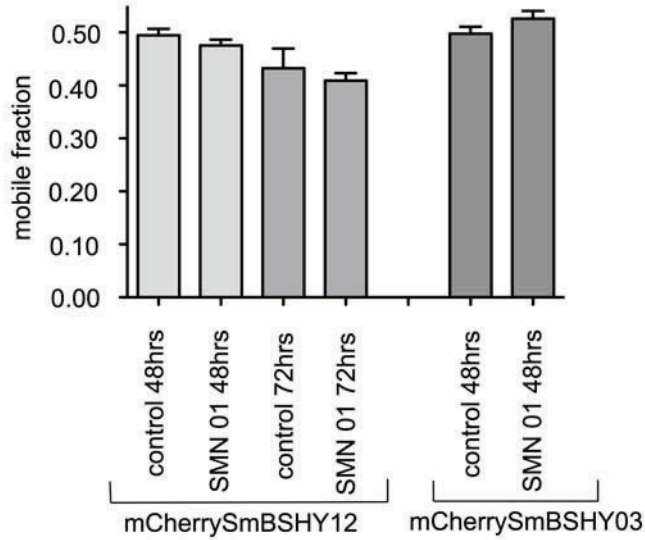

E

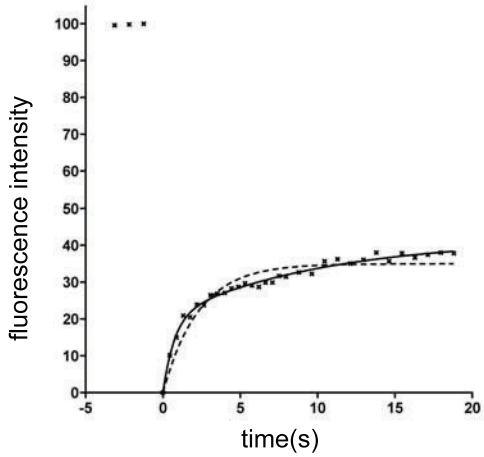

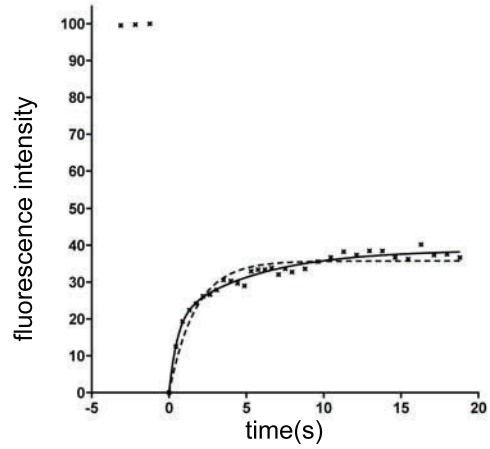

F